
REX: CAUSAL DISCOVERY BASED ON MACHINE LEARNING AND EXPLAINABILITY TECHNIQUES

Jesús Renero^{1,3}, Roberto Maestre^{1,3}, and Idoia Ochoa^{2,3}

¹BBVA Madrid, Spain

²Tecnun, University of Navarra, San Sebastián, Spain

³Instituto de Ciencia de Datos e Inteligencia Artificial (DATAI), University of Navarra, Pamplona, Spain

January 23, 2025

ABSTRACT

Explainability techniques hold significant potential for enhancing the causal discovery process, which is crucial for understanding complex systems in areas like healthcare, economics, and artificial intelligence. However, no causal discovery methods currently incorporate explainability into their models to derive causal graphs. Thus, in this paper we explore this innovative approach, as it offers substantial potential and represents a promising new direction worth investigating. Specifically, we introduce REX, a causal discovery method that leverages machine learning (ML) models coupled with explainability techniques, specifically Shapley values, to identify and interpret significant causal relationships among variables.

Comparative evaluations on synthetic datasets comprising continuous tabular data reveal that REX outperforms state-of-the-art causal discovery methods across diverse data generation processes, including non-linear and additive noise models. Moreover, REX was tested on the Sachs single-cell protein-signaling dataset, achieving a precision of 0.952 and recovering key causal relationships with no incorrect edges. Taking together, these results showcase REX’s effectiveness in accurately recovering true causal structures while minimizing false positive predictions, its robustness across diverse datasets, and its applicability to real-world problems. By combining ML and explainability techniques with causal discovery, REX bridges the gap between predictive modeling and causal inference, offering an effective tool for understanding complex causal structures. REX is publicly available at <https://github.com/renero/causalgraph>.

Keywords: Causal Discovery, Explainability, Shapley Values

1 Introduction

Causal discovery —the process of identifying cause-and-effect relationships from observational data— is a pivotal challenge in artificial intelligence (AI) and machine learning. Unveiling causal structures enables robust predictions, facilitates counterfactual reasoning, and enhances decision-making processes in complex systems [1]. Traditional methods for causal discovery often rely on statistical tests for independence and structural equation modeling, which may not scale efficiently with high-dimensional data or effectively capture intricate non-linear relationships [2, 3].

In recent years, machine learning models, particularly deep learning architectures, have achieved remarkable success in predictive tasks. However, these models are typically considered “black boxes” due to their lack of interpretability. This opacity has led to a growing interest in explainable AI (XAI) techniques, with Shapley values emerging as a prominent method for interpreting model predictions [4]. Shapley values, grounded in cooperative game theory, provide a principled approach to attributing the contribution of each feature to the output of a model by quantifying the average marginal contribution of a feature across all possible subsets of features [5].

While Shapley values offer valuable insights into feature importance within a model’s predictive framework, the link between feature importance and causal influence is non-trivial. A high Shapley value for a feature indicates a strong

impact on the model’s predictions but does not necessarily imply a direct causal relationship with the target variable [6, 7]. Moreover, correlations captured by the model may be confounded by hidden variables or represent spurious associations [1]. Therefore, leveraging Shapley values for causal discovery requires careful consideration to avoid misleading inferences.

Despite the advancements in both causal discovery and explainable AI, there is a notable absence of methods that integrate explainability techniques—specifically Shapley values—into the causal discovery process to extract causal graphs. This highlights a significant gap in the intersection of these two fields, offering a promising new direction.

In this paper, we propose a novel method coined REX that integrates Shapley values into the causal discovery process, aiming to uncover causal structures by interpreting feature attributions from machine learning models. By cautiously exploiting the conceptual connection between Shapley values and causal relationships, REX helps narrow down the set of features that play significant roles in the causal graph. This targeted approach allows us to focus on the most influential variables for further causal analysis, improving the efficiency and accuracy of causal discovery in complex datasets.

We demonstrate REX’s competitive performance on synthetic datasets traditionally employed to evaluate new models, encompassing diverse generation processes, as well as on a complex real-world dataset. This performance underscores its practical applicability and the advantages over existing methods in addressing real-world causal discovery challenges. By integrating explainability techniques into causal discovery, we contribute to bridging the gap between predictive modeling and causal inference—a topic of increasing importance in the AI community [8, 9, 10]. This integration not only enhances the interpretability of causal models but also improves the identification of causal relationships by focusing on features with significant contributions.

1.1 Related work

Classical approaches to causal discovery are primarily divided into three families: constraint-based methods, score-based methods, and structural causal models (SCMs).

Constraint-based methods, such as the PC algorithm [2] and Fast Causal Inference (FCI) [11], rely on conditional independence tests to infer causal structures. These methods explore statistical dependencies in the data to determine causal relationships between variables.

Score-based methods, like Greedy Equivalence Search (GES) [12], search for the model that best fits the data according to a scoring criterion. This approach involves evaluating different graph structures and selecting the one that optimizes an objective function, balancing model fit and complexity.

Structural causal models (SCMs) provide a framework for representing and estimating causal relationships through equations that describe how variables influence one another [1]. Within this category, the LiNGAM algorithm [13] exploits non-Gaussianity in data to identify causal structures in linear models, assuming linear, non-Gaussian, acyclic relationships. Causal Additive Models (CAM) [14] extend these methods by modeling nonlinear relationships using additive noise models, allowing for high-dimensional order search and penalized regression techniques. However, these models often require strong assumptions about the data-generating process and may struggle with complex nonlinearities inherent in real-world data [3].

Hybrid methods combine elements of both constraint-based and score-based approaches to improve accuracy and computational efficiency [15]. These methods aim to leverage the strengths of each approach to overcome individual limitations.

Recent advancements have led to the application of machine learning techniques in causal discovery. Algorithms like NOTEARS [16] and Structural Agnostic Modeling (SAM) [17] formulate causal discovery as continuous optimization problems, enabling the use of gradient-based methods to learn directed acyclic graphs (DAGs). SAM, in particular, employs adversarial learning to model causal structures without making strong assumptions about the data distribution. These methods improve scalability and can capture nonlinear relationships but may still face challenges related to interpretability and computational demands [18].

2 Preliminaries

Causal discovery aims to infer cause-effect relationships between variables in observational data, typically represented by a causal graph. A causal graph, often modeled as a Directed Acyclic Graph (DAG), consists of nodes representing variables and directed edges indicating causal influences. The primary challenge in causal discovery is to identify

these causal relationships without direct evidence from interventions, relying instead on specific assumptions about the data and its underlying generative processes.

Let $\mathbf{X} = \{X_1, X_2, \dots, X_p\}$ represent a vector of p continuous variables, with unknown joint probability distribution $P(\mathbf{X})$. The observational causal discovery setting considers m independent and identically distributed (iid) samples drawn from $P(\mathbf{X})$. The goal is then to infer the *causal DAG* $\mathcal{G} = (V, E)$, where V is the set of variables and E is the set of directed edges ($X_j \rightarrow X_i$) representing the causal relationship “ X_j causes X_i ”.

The *Causal Markov Condition (CM)* states that, given the causal graph \mathcal{G} , the joint probability distribution $P(\mathbf{X})$ factorizes as:

$$P(X_1, X_2, \dots, X_n) = \prod_{i=1}^p P(X_i | \text{pa}(i, \mathcal{G})), \quad (1)$$

where $\text{pa}(i, \mathcal{G})$ represents the parents of X_i in the graph. In other words, the CM states that, given a causal graph, each variable is conditionally independent of its non-descendants, given its parents in the graph. This condition is crucial for causal inference as it ensures that the relationships in the graph can be used to explain the dependencies in the data.

Faithfulness refers to the assumption that all conditional independencies present in the observed data are reflected in the structure of the causal graph. Formally, the distribution P in Eq. (1) is said to be faithful to \mathcal{G} if the only conditional independencies in P are those implied by the d-separation in \mathcal{G} [2, 1]. This assumption ensures that there are no accidental independencies in the data due to parameter values (e.g., when causal effects perfectly cancel each other out).

Faithfulness, combined with the Causal Markov Condition, is essential for inferring the correct causal structure from observational data, as it guarantees that the observed statistical relationships correspond directly to the structure of the causal graph. Additionally, in the causal discovery setting, the underlying model that generates the data is assumed to be a general Structural Equation Model (SEM) as follows:

$$X_i = f_i(X_{\text{pa}(i, \mathcal{G})}, \varepsilon_i), \text{ with } \varepsilon_i \sim \mathcal{N}(0, 1), \text{ for } i = 1, \dots, p, \quad (2)$$

where f_i is a function from $\mathbb{R}^{|\text{pa}(i, \mathcal{G})|+1} \rightarrow \mathbb{R}$, and ε_i is a unit centered Gaussian noise. SEM is a framework for modeling causal relationships where each variable is expressed as a function of its direct causes (parents) and an error term, typically assumed to be independent noise. SEMs are also essential for causal discovery because they provide a formal way to represent and quantify the effects of interventions and establish the relationships between variables.

2.1 SHAP values and causal relationships

In a causal context, if a feature does not significantly change the prediction of a target variable when added to a subset of other features, it may indicate conditional independence between the feature and the target variable, given that subset. This idea aligns with causal inference, where identifying conditional independence is key to determining whether a variable has a direct causal effect or if the relationship is mediated by other variables. By interpreting Shapley values in this way, we can gain insights into the underlying causal relationships, although Shapley values alone do not establish causality.

Several studies have explored the potential connections between SHAP values and causal relationships among variables [19, 20, 21]. These papers suggest that while SHAP values, derived from cooperative game theory, are primarily used for model explainability by attributing the contribution of each feature to a model’s prediction, they may also have implications for understanding causal relationships. However, as mentioned in Section 1, it is important to emphasize that SHAP values themselves are not inherently causal. They do not establish causal relationships but can be used in conjunction with causal inference techniques to gain insights into potential causal dynamics within the data. This area of research is ongoing, and while promising, it is crucial to distinguish between correlation, as typically highlighted by SHAP values, and causation, which requires more rigorous methodological approaches.

2.2 Mathematical Foundation

In this section, we establish the theoretical connection between Shapley values and conditional independence within the context of causal discovery. This foundation supports the use of Shapley values in identifying causal relationships by relating feature importance measures to probabilistic dependence structures.

Let F be the set of all features (variables), excluding the target variable X_i . Each feature $X_j \in F$ is considered a “player” in a cooperative game where the objective is to predict X_i . We define a function $\hat{f}(S) : 2^{|F|} \rightarrow \mathbb{R}$ that maps a subset of features $S \subseteq F$ to a real number representing the contribution of S to predicting X_i , with $|F|$ being the

cardinality of F . The, the Shapley value ϕ_j for feature X_j is defined as:

$$\phi_j = \sum_{S \subseteq F \setminus \{X_j\}} \frac{|S|! (|F| - |S| - 1)!}{|F|!} \left[\hat{f}(S \cup \{X_j\}) - \hat{f}(S) \right], \quad (3)$$

where $\hat{f}(S \cup \{X_j\}) - \hat{f}(S)$ represents the marginal contribution of feature X_j to the prediction of X_i given subset S .

2.2.1 Marginal Contributions and Conditional Independence

In [22], a connection between Shapley value summands and conditional independence is demonstrated by relating conditional independence in a faithful Bayesian network with the summands of the Shapley value. Specifically, within this framework, if a variable X_j provides additional information about the target variable given a subset S of other variables, this relationship is captured by the Shapley value summands for X_j given S . This interpretation aligns with the concept of conditional independence, where the Shapley summand reflects the additional predictive contribution of X_j in the context of S . In causal discovery, assuming causal sufficiency and faithfulness, SHAP values can indicate conditional independence relationships within a causal DAG, providing an interpretable approach to uncovering causal relationships rather than mere associations.

To connect Shapley values with conditional independence, consider the marginal contribution $\delta_{j,S}$ of feature X_j for a specific subset $S \subseteq F \setminus \{X_j\}$, given by $\delta_{j,S} = \hat{f}(S \cup \{X_j\}) - \hat{f}(S)$. Assuming that $\hat{f}(S)$ accurately reflects the predictive power of S for X_i , the marginal contribution $\delta_{j,S}$ relates to the conditional dependence between X_i and X_j given S . Specifically:

- If X_j provides no additional information about X_i given S , then X_i is conditionally independent of X_j given S , denoted as $X_i \perp\!\!\!\perp X_j \mid S$. In this case $p(X_i \mid X_j, S) = p(X_i \mid S)$, and the marginal contribution is zero ($\delta_{j,S} = 0$).
- If X_j provides additional predictive information about X_i given S , then X_i is conditionally dependent on X_j given S , denoted as $X_i \not\perp\!\!\!\perp X_j \mid S$. In this case:

$$p(X_i \mid X_j, S) \neq p(X_i \mid S), \quad (4)$$

and the marginal contribution is positive ($\delta_{j,S} > 0$).

2.2.2 Aggregating Over All Subsets

The Shapley value ϕ_j aggregates the marginal contributions $\delta_{j,S}$ over all subsets S of $F \setminus \{X_j\}$, weighted by the Shapley weights:

$$w(S) = \frac{|S|! (|F| - |S| - 1)!}{|F|!}. \quad (5)$$

These weights satisfy $\sum_S w(S) = 1$ and reflect the importance of each subset in the calculation.

2.2.3 Relating Shapley Values to Conditional Dependence

To formalize the relationship between Shapley values and conditional independence, we introduce the indicator function $I_{j,S}$:

$$I_{j,S} = \begin{cases} 1, & \text{if } p(X_i \mid X_j, S) \neq p(X_i \mid S), \\ 0, & \text{if } p(X_i \mid X_j, S) = p(X_i \mid S). \end{cases} \quad (6)$$

Using this indicator function, the Shapley value ϕ_j can be expressed as:

$$\phi_j = \sum_S w(S) \cdot \delta_{j,S} = \sum_S w(S) \cdot I_{j,S} \cdot \delta_{j,S}. \quad (7)$$

Assuming that the average marginal contribution $\bar{\delta}_j$ is approximately constant across subsets where X_j is conditionally dependent on X_i , we can approximate ϕ_j as:

$$\phi_j \approx \bar{\delta}_j \cdot \sum_S w(S) \cdot I_{j,S}. \quad (8)$$

2.2.4 Weighted Probability of Conditional Dependence

The term $\sum_S w(S) \cdot I_{j,S}$ represents the weighted probability that X_j is conditionally dependent on X_i across all subsets S , under the probability distribution defined by the Shapley weights $w(S)$, i.e.,:

$$P_{\text{weighted}}(X_j \text{ is conditionally dependent on } X_i) = \sum_S w(S) \cdot I_{j,S}. \quad (9)$$

Thus, the Shapley value ϕ_j can be interpreted as:

$$\phi_j \approx \bar{\delta}_j \cdot P_{\text{weighted}}(X_j \text{ is conditionally dependent on } X_i). \quad (10)$$

This approximation indicates that the Shapley value ϕ_j is proportional to both: i) the average strength of the dependence ($\bar{\delta}_j$); and ii) the weighted probability that X_j is conditionally dependent on X_i .

2.2.5 Implications for Causal Discovery

The relationship between Shapley values and conditional dependence suggests that features with higher Shapley values are more likely to be conditionally dependent on the target variable X_i , while features with lower Shapley values are more likely to be conditionally independent. This connection provides a theoretical justification for using Shapley values in causal discovery.

More formally, a high Shapley Value (ϕ_j large) indicates that X_j frequently contributes significant predictive information about X_i across various subsets S , suggesting a potential causal relationship or strong association. On the contrary, a low Shapley Value (ϕ_j small) implies that X_j rarely provides additional predictive information about X_i , indicating possible conditional independence and a lower likelihood of a direct causal link.

By leveraging this theoretical foundation, it is correct to utilize Shapley values to estimate the conditional dependence structure among variables. However, it is important to acknowledge the assumptions underlying this connection:

- The approximation given in Eq. (10) assumes that $\bar{\delta}_j$ is relatively consistent across subsets where X_j is conditionally dependent on X_i .
- In practice, the marginal contributions $\delta_{j,S}$ may vary significantly across different subsets S , and the assumption of a constant $\bar{\delta}_j$ serves as a simplifying approximation.
- The predictive function $\hat{f}(S)$ is assumed to accurately capture the true conditional probabilities $p(X_i | S)$.
- To interpret SHAP values in a causal discovery context, two core assumptions need to be assumed: faithfulness and causal sufficiency. These assumptions are essential to ensure that the inferred relationships are not merely statistical dependencies but can be interpreted as causal connections in the resulting causal DAG.

Despite these assumptions, the established relationship provides valuable insights into how Shapley values can reflect the underlying conditional independence structures, supporting their use in causal inference tasks.

3 Proposed method

The proposed method REX approaches the causal discovery problem in a series of steps (see Fig. 1). First, we fine-tune and train a series of regressors to predict each variable X_i , for $i = 1, \dots, p$, using the remaining $p - 1$ variables in the dataset, denoted as $X_{\setminus i} = \{X_1, \dots, X_{i-1}, X_{i+1}, \dots, X_p\}$. Once the regressors are fine-tuned and trained, we compute Shapley values to estimate the contribution of each variable to the prediction, applying a bootstrapping mechanism, i.e., iteratively using different samples of the dataset. Through this repeated sampling, REX identifies a robust set of features that can be considered the potential causes (i.e., $pa(X_i)$) for each target variable X_i . As a final step, results from the different regressors are combined to obtain a plausible causal graph, which is reviewed to direct edges and remove eventual cycles. Next, we describe these steps in detail.

3.1 Models training

The first step in deriving the causal model is to train a separate model to predict each variable in the dataset, with hyperparameter optimization (HPO). Before model training, the data is normalized by removing the mean and scaling to unit variance. To ensure robustness, we employ two complementary regressors: a deep feed-forward neural network (DFN) and gradient boosting trees (GBT). DFNs are highly flexible models capable of approximating any function, leveraging their capacity as universal approximators, as demonstrated by [23]. GBTs, known for their effectiveness in handling

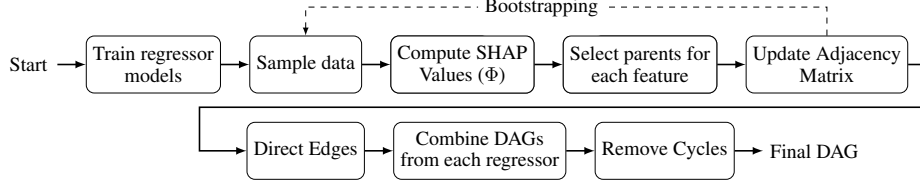


Figure 1: Summary of the different steps performed by REX.

tabular continuous data and offering more interpretable outputs as shown in [24], serve to validate and complement the results obtained from the DFN models, with the XGBoost implementation used in this study. Although the REX framework allows for the integration of additional regressors, the results from DFN and GBT have proven to be sufficiently robust for our purposes.

A total of p DFN and p GBT models are trained, where the target variable is feature X_i , for $i = 1, \dots, p$, and the input data consists of the remaining variables $X_{\setminus i}$. The DFN models include an additional additive noise variable $\varepsilon \sim \text{Uniform}(0, 1)$ as input, which is re-generated at each training forward step. Each DFN and GBT model is trained with mean squared error (MSE) as loss function. These models act therefore as functions \hat{f}_i that map inputs $X_{\setminus i}$ to the estimate of the corresponding X_i , i.e., $\hat{f}_i(X_{\setminus i}, \varepsilon_i) = \hat{X}_i \approx X_i$.

The model hyperparameters are determined in the training phase for each dataset, using a tree-structured Parzen estimator (TPE) [25] with an 80/20 split for train and validation. Hyperparameter optimization is a critical step, as one of the assumptions stated in Section 2.2.5 is that regressor \hat{f} accurately captures the true conditional probabilities.

3.2 Bootstrapping and Initial Causal Graph Construction

In this phase, we implement the bootstrapping approach to construct an initial undirected causal graph. This process involves three main steps: computing SHAP values to assess feature importance, selecting potential parent features based on their impact, and updating an adjacency matrix that represents candidate causal connections. These steps are iteratively repeated in the bootstrapping loop (Algorithm 1) to build a stable causal structure.

Algorithm 1 Bootstrapped DAG construction

Require: Let \hat{f} be a regressor model, fine tuned –DFN or GBT.

- 1: Initialize an empty adjacency matrix $\mathbf{A} \in \mathbb{R}^{p \times p}$.
- 2: **for** $t = 1$ to T (nr. of bootstrapping iterations) **do**
- 3: Sample a subset of data $\mathbf{X}^{(t)}$ from \mathbf{X} (observational data).
- 4: **for** each feature X_i **do**
- 5: Fit SHAP explainer with $\mathbf{X}_{\setminus i}^{(t)}$ and model \hat{f} , to obtain $\Phi^{(i)} = \{\phi_1 \dots \phi_{i-1}, \phi_{i+1} \dots \phi_p\}$
- 6: Run Algorithm 2 with $\Phi^{(i)}$ to obtain $pa(X_i)$
- 7: **for** each pair of adjacent features $(X_i, X_j \in pa(X_i))$ **do**
- 8: Increment the corresponding entry in \mathbf{A} :

$$a_{i,j} \leftarrow a_{i,j} + 1$$
- 9: **end for**
- 10: **end for**
- 11: **end for**
- 12: Normalize \mathbf{A} by T : $a_{i,j} \leftarrow \frac{a_{i,j}}{T}$
- 13: Filter edges in \mathbf{A} : $a_{i,j} \leftarrow 0$ if $a_{i,j} < \tau$
- 14: **return** Adjacency matrix \mathbf{A} representing the causal graph

3.2.1 Computing SHAP Values for Feature Impact

The first step in Algorithm 1, after sampling a subset of the data, is to compute SHAP values for each feature to identify its impact on the target variable in each regressor model. For a given model (DFN or GBT), the SHAP value ϕ_j is calculated for each feature X_j when predicting the target variable X_i . This value indicates the marginal contribution of X_j to the prediction of X_i , allowing us to interpret $\phi_j > 0$ as evidence that X_j is likely to influence X_i (i.e., $X_i \not\perp\!\!\!\perp X_j$). This computation provides a foundation for identifying variables that may play a causal role in influencing each target variable, as described in Section 2.2.5.

Algorithm 2 Parents selection from SHAP values

Require: Input array $\Phi = \{\phi_1 \dots \phi_{p-1}\}$, SHAP values

- 1: $\Delta \leftarrow$ Pairwise Euclidean distances in Φ
- 2: $\Delta' \leftarrow$ Sort diffs in Δ in descending order
- 3: Initialize ε to $\max(\Delta) + \text{constant}$
- 4: **repeat**
- 5: Run DBSCAN on Φ with parameter ε
- 6: $n \leftarrow$ Number of clusters
- 7: **if** $n = 1$ **then**
- 8: $\varepsilon \leftarrow \varepsilon - \max(\Delta')$
- 9: Remove $\max(\Delta')$ from Δ'
- 10: **end if**
- 11: **until** $n > 1$ or $\Delta' = \emptyset$
- 12: **if** No clusters formed **then**
- 13: **return** None
- 14: **else**
- 15: **return** Features in cluster with highest mean SHAP value
- 16: **end if**

3.2.2 Parents Selection

In the second step of Algorithm 1, we apply the DBSCAN clustering algorithm to group features based on their SHAP values and select those that have a significant impact on predicting the target variable. Feature clusters are adjusted dynamically by decreasing the neighborhood radius parameter ε until more than one group are detected, helping to separate influential features from less impactful ones. This clustering process effectively selects potential parent features, as it isolates variables that likely have causal influence on the target. Algorithm 2 outlines this clustering procedure in detail, and Appendix A describes the process with a visual example and additional details.

Simpler heuristic methods, such as using average SHAP values with percentile thresholds, were explored but produced worse results, as they struggled to effectively distinguish between features with varying levels of impact.

3.2.3 Adjacency Matrix Update and Graph Construction

With the influential features identified, we proceed to construct an initial causal graph by updating an adjacency matrix, which records candidate edges between features. In each bootstrapping iteration, a subset of the data $\mathbf{X}^{(t)}$ is sampled, and SHAP-based parent selection is performed. For each pair of selected features, the corresponding entry in the adjacency matrix \mathbf{A} is incremented, capturing the frequency of selection across iterations. After bootstrapping, we apply a threshold τ to filter out edges with low frequencies, retaining only stable and meaningful connections. This thresholding process yields a plausible undirected causal graph, representing the initial structure without directed edges.

The percentage of rows to be selected (step 3 in Algorithm 1) is set to be $\geq 1 - q^{1/r}$, where q is the maximum acceptable probability that any given row is not selected in any iteration (typically $q = 0.01$), and r is the number of iterations defined for the bootstrapping mechanism (typically $r = 100$).

3.3 Directing edges

The direction of each edge in the graph is established based on the method proposed by the Additive Noise Model (ANM) for structure identification as described in [3] and improved in [26]. This procedure is applied to each un-oriented edge by fitting a regression model (either a Gaussian Process Regressor (GPR) or a Generalized Additive Model (GAM)) to approximate the dependent variable (X_j) as a function of the predictor (X_i) plus Gaussian noise. This process is repeated in the reverse direction, with X_i as the dependent variable and X_j as the predictor, for each selected pair of features.

To determine whether the variables are conditionally independent, we use the Hilbert-Schmidt Independence Criterion (HSIC) [27], specifically testing for independence between the residuals of the regression and the predictor variable. We adopt the Gaussian kernel for the HSIC independence test, which uses the median distance as the bandwidth, guaranteeing consistency in the test [28]. If the independence hypothesis is accepted, we infer that the causal direction is from the predictor to the dependent variable.

The resulting graph is a directed acyclic graph (DAG) that captures the inferred causal relationships between the features.

3.4 Final DAG

The methodology presented here culminates in the generation of the final DAG, denoted as \mathcal{G}_{REX} . This final DAG is produced by taking the union (\cup) of the two DAGs \mathcal{G}_{DFN} and \mathcal{G}_{GBT} , which are generated by the described procedure when using DFN and GBT as the regressors, respectively (see Appendix C for a performance comparison among \mathcal{G}_{REX} , \mathcal{G}_{DFN} and \mathcal{G}_{GBT}).

The final DAG \mathcal{G}_{REX} must be acyclic to represent valid causal relationships. Hence, in those cases where the new proposed DAG contains cycles or bidirectional edges between two nodes, as a result of the union of two DAGs, we employ a strategy based on the use of the *SHAP discrepancy* $\delta_j^{(i)}$ to make it acyclic.

The SHAP discrepancy is introduced as a measure to assess how well the Shapley values of a feature explain the variability in the target variable. It quantifies the extent to which the contributions of a feature X_j (captured by its Shapley values ϕ_j) align with the actual values of X_i (see Appendix B for more details), computed as follows:

$$\delta_j^{(i)} = 1 - R^2(X_i, \phi_j) = \frac{\sum_{k=1}^m (x_{k,i} - \phi_{k,j})^2}{\sum_{k=1}^m (x_{k,i} - \bar{X}_i)^2}, \quad (11)$$

where $x_{k,i}$ is the k -th observation of X_i , $\phi_{k,j}$ is the corresponding Shapley value of X_j for predicting X_i , \bar{X}_i is the mean of X_i , and m is the total number of samples.

A lower SHAP discrepancy indicates that the Shapley values ϕ_j closely approximate X_i , suggesting a stronger potential causal influence from X_j to X_i . In the context of removing cycles in the DAG, the SHAP discrepancy helps identifying which edges are less supported by the data. Briefly, when a cycle is detected, edges with higher discrepancies are considered for reorientation or removal to break the cycle, ensuring the resulting graph accurately represents the underlying causal relationships.

The proposed method iteratively examines each detected cycle and seeks to resolve it by removing edges with the highest SHAP discrepancy. In particular, for each cycle, the proposed strategy computes the SHAP discrepancies for each edge in the cycle. By comparing these discrepancies, it identifies edges that could reduce the overall discrepancy by reversing their direction, indicating potential misorientations. Reorienting such edges can break the cycle while preserving the causal relationships suggested by the data. If reorientation is insufficient or not possible, the proposed method removes the edge with the largest SHAP discrepancy—implying it is the weakest link in the cycle—to eliminate the cyclicity.

This process ensures that the final graph is acyclic and retains the most significant causal structures inferred from the data. The algorithm effectively balances the need to break cycles with the goal of maintaining the integrity of the underlying causal relationships.

3.5 Visual example

The intermediate DAGs obtained by REX are summarized, in a simplified way, in Fig. 2. Each of the regressors tuned and trained to predict each of the variables in the dataset (Section 3.1) are used to compute SHAP values (Section 3.2.1), and from them, select the candidate parents (causes) of each variable (Section 3.2.2). Running SHAP from the trained models to select parents is done following a bootstrap approach, by sampling different portions of the data at each iteration to fit the selected Shapley explainer. After that, a filtered adjacency matrix (Section 3.2.3) is used to outline an unoriented graph, for each of the two regressors (Fig. 2a,b). As a next step, the unoriented graphs become directed graphs (Fig. 2c,d), by using ANM (HSIC) (Section 3.3). These may contain edges that do not exist in the true DAG (e.g., $B \leftarrow C$ in (c)), or wrongly directed edges (e.g., $E \leftarrow C$ in (c) and $D \rightarrow C$ in (d)). The union of these two graphs results in the graph depicted in Fig. 2e, where all edges found by any one of the regressors are included. However, this union operation may result in some double-directed edges and cycles (e.g., $C \leftrightarrow D$, $C \leftrightarrow E$ and $B \rightarrow D \rightarrow C \rightarrow B$ in (e)) that need to be resolved (Section 3.4) to produce the final DAG (Fig. 2f).

4 Results on synthetic data

We first consider synthetic data for the evaluation, as it allows to operate under controlled assumptions, where the causal structure is fully specified, and the data generation process is explicitly governed by known structural equations. Consequently, there are no unobserved confounders, fulfilling the causal sufficiency assumption, and the structural

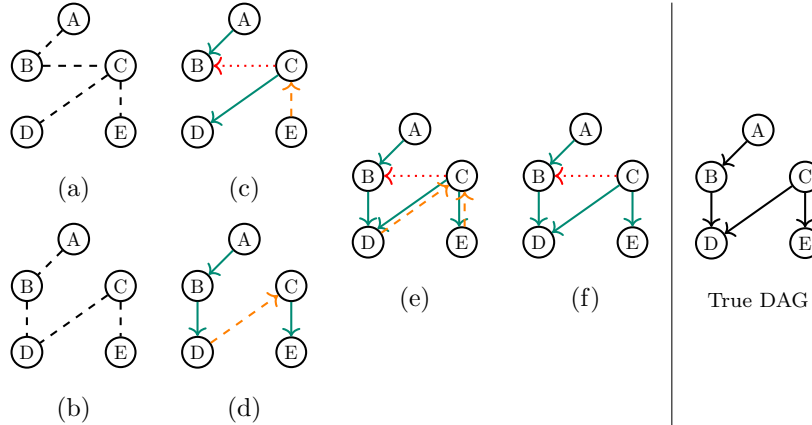


Figure 2: A visual summary of the intermediate graphs generated by REX to obtain the final DAG \mathcal{G}_{REX} . (a)-(b) represent the unoriented graphs for each of the two regressors after running the steps described in Sections 3.1, 3.2.1, 3.2.2 and 3.2.3. (c)-(d) are the result of establishing the direction of each edge presented in (a)-(b), respectively, following the approach described in Section 3.3. (e) is the initial DAG resulting from the union of DAGs (c)-(d). (f) is final DAG \mathcal{G}_{REX} resulting from removing cycles and/or bidirectional edges from (e), following the steps described in Section 3.4. The true DAG is also depicted for comparison. Green arrows represent correctly predicted edges, orange ones edges with the incorrect direction, and red ones edges that are missing in the true DAG.

Table 1: Average and standard deviation number of edges in the generated DAGs for $p = 10, 15, 20, 25$.

Nr of features	10	15	20	25
Nr of edges in ground truth	15 ± 5.5	23 ± 7.62	33 ± 6.47	42 ± 10.31

equations are stable under interventions. Additionally, the data respects the faithfulness assumption, ensuring that all observed conditional independencies align with the causal structure of the DAG.

We conducted experiments using five families of synthetic datasets, each corresponding to a specific type of causal relationship: linear, polynomial, sigmoid additive, Gaussian additive, and Gaussian mixed models. These datasets vary in complexity and non-linearity, and were generated following the methodology described in [29] and [30].

For each synthetic generation mechanism family, we generated datasets with $p = 10, 15, 20$ and 25 variables, each containing $m = 500$ samples (see Table 1 for details on the distribution of number of edges in the ground truth DAGs). For a robust and reliable evaluation, 10 different datasets were generated for each combination of mechanism family and variable count, resulting in 200 datasets (5 families $\times 4$ variable counts $\times 10$ datasets). All synthetic datasets used to benchmark REX in this study have been made available in the GitHub repository, along the parametrization used for REX and compared methods.

These datasets, together with their corresponding unique ground truth DAGs, are used to benchmark REX against the state-of-the-art causal discovery methods (hereafter referred to as *compared methods*) PC [2], NOTEARS [16], GES [12], LiNGAM [13], FCI [11], and CAM [14]. NOTEARS was trained and thresholded with the optimum value found for all datasets used in the study. The rest of the methods have been used with default parametrization.

All computations were performed on a system equipped with an Apple M2 Pro processor and 32 GB of RAM, without the use of parallelization or GPU acceleration.

4.1 Evaluation metrics

To compare a predicted Directed Acyclic Graphs (DAG) against a ground truth DAG, we first compute the True Positives (TPs), False Positives (FPs), and False Negatives (FNs). We define a TP as an edge with the correct direction in both the predicted and ground truth DAGs; a FP as an inferred edge that is not present, or has the opposite direction, in the ground truth DAG; and a FN as an edge present in the ground truth but missing or misoriented in the predicted DAG. Note that a true edge inferred but with the opposite direction is counted both as a FP and a FN. With these metrics, we then compute standard graph-based metrics: precision, recall, and F1-score. Precision is the ratio of

correctly predicted edges (TPs) to all predicted edges (TPs + FPs), recall is the proportion of true edges recovered in the predicted DAG (i.e., $TPs/(TPs+FNs)$), and the F1-score is the harmonic mean of precision and recall. We also consider the difference in the number of edges between the predicted DAG and the true DAG, to evaluate whether a method tends to over- or under-estimate the number of edges.

Additionally, we calculate the Structural Hamming Distance (SHD) [15], which measures the difference between two DAGs by counting missing or extraneous edges, and Structural Intervention Distance (SID) [31], which evaluates how closely two DAGs agree on causal inference statements derived from interventions. Unlike SHD, SID focuses purely on the causal implications of the graph structure, making it particularly suitable for assessing causal discovery algorithms.

A high-performing DAG will demonstrate high precision, recall, and F1, alongside low SHD and SID values.

4.2 Experimental Results

We first assess REX as a function of the number of variables p , across the five considered families of synthetic datasets, to evaluate its performance with increasingly complex datasets.

Looking at the F1 score (Fig. 3a), we observe that REX achieves high predictive performance, especially for lower and moderate values of p , with median F1 scores consistently above 0.7. This reflects REX’s capacity to balance precision and recall effectively in identifying causal relationships. Although some variability is present, the high F1 scores across different values of p underscore REX’s robustness. However, there is a slight decrease in the median F1 score for the highest value of p , suggesting that scalability might pose a limitation to its predictive power in very high-dimensional settings.

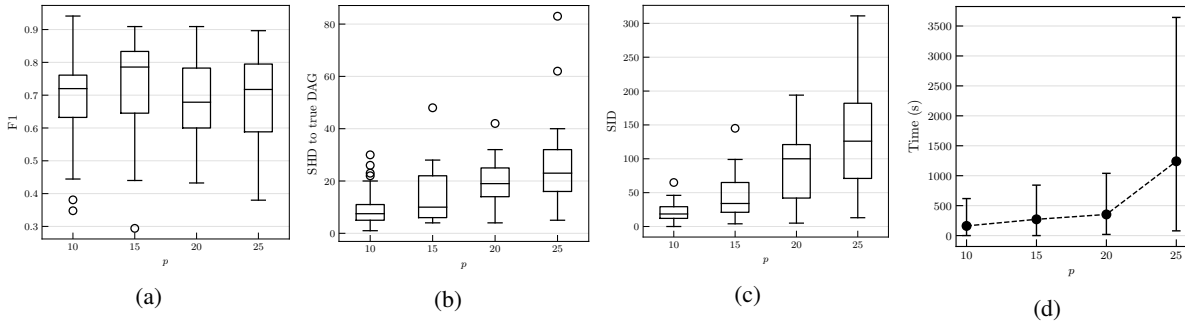


Figure 3: Effect of increasing the number of variables in the input dataset with REX in the following metrics: (a) F1 score; (b) SHD; (c) SID; and (d) computation time. Results are computed for the five considered families of synthetic data.

In terms of SHD (Fig. 3b), REX exhibits relatively low SHD values, with a concentrated distribution, particularly for smaller values of p . This suggests that REX maintains structural accuracy effectively, even as the dimensionality grows. However, there is a noticeable upward trend in SHD for larger values of p , indicating that while REX performs well in smaller graphs, its structural precision may gradually decrease as the dimensionality increases. As for SID (Fig. 3c), we also see remarkable low values for lower p and a similar trend to that shown for SHD, as the number of variables increases.

Next, we evaluate the computation time (Fig. 3d), showing that REX’s time requirements increase as p grows, which is an expected outcome given the combinatorial nature of SHAP values computation. While the computational cost becomes more significant at higher values of p , the performance remains reasonable for moderate-dimensional datasets. Users should be aware that runtime will increase substantially with higher-dimensional data, indicating a potential challenge in scalability.

Overall, REX demonstrates strong performance in terms of structural accuracy and F1 score, especially for small to medium-sized datasets, maintaining computational demands and structural precision acceptable for moderate values of p .

4.2.1 Results by synthetic dataset

When evaluating these metrics per synthetic dataset family (see Appendix E, Fig. 12), we do not observe significant differences. The results indicate that REX performs robustly across a range of complexities in data structure, showing consistent trends across various settings.

REX achieves high F1 scores (Fig. 12a) across all dataset families, with particularly strong performance in the Gaussian (additive), Gaussian (mixed), and Sigmoid (additive) families, where F1 scores remain above 0.6 even as p increases. In contrast, the Linear and Polynomial datasets show more variability, particularly at higher p values, indicating greater difficulty for REX in these simpler structures. Precision and recall (Fig. 12b,c) follow similar trends, with consistently high values in the Gaussian and Sigmoid families, reflecting REX’s ability to capture relevant causal relationships effectively. Linear and Polynomial datasets, however, show greater variability, suggesting that REX may struggle with these structured relationships at higher dimensionalities.

The SHD and SID metrics (Fig. 12d,e) reinforce these findings, with low values in Gaussian and Sigmoid families, indicating REX’s accuracy in reconstructing causal structures and capturing correct causal directions. Higher values in Linear and Polynomial datasets, particularly as p increases, suggest occasional challenges in directionality and structure for these settings.

Training time (Fig. 12f) increases with p across all families, as expected. REX requires less time on Linear and Polynomial datasets compared to Gaussian and Sigmoid, likely due to the simpler relationships in these structures.

4.2.2 Comparison with other methods

Next, we compare REX against the compared methods (see also Appendix D for sample DAGs generated by each method). We observe that REX consistently shows strong performance, particularly in F1 score (Fig. 4a), where it achieves higher values relative to most other methods. Notably, REX exhibits a lower variance than the other methods, with values tightly concentrated around the median. This stability across metrics suggests that REX is less sensitive to variations in the data, resulting in more consistent performance. As suggested by the obtained F1 scores, REX stands out in aligning well with the true number of edges in the causal graph (Fig. 4b), indicating its effectiveness at avoiding both excessive edge predictions (false positives) and missing edges (false negatives). Compared to other methods, it exhibits a narrower interquartile range, implying lower variability in edge prediction across different datasets. This consistency suggests a robustness in REX’s performance, with fewer instances of significant deviations from the true edge count.

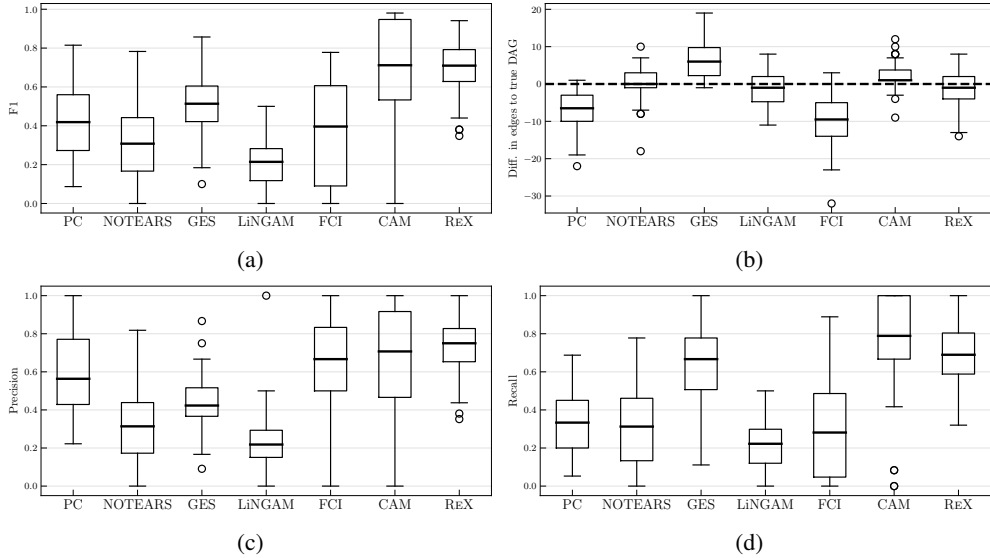


Figure 4: Comparative performance of REX against the benchmark methods PC, NOTEARS, GES, LiNGAM, FCI, and CAM across four key metrics: (a) F1 score; (b) edge difference, (c) precision; and (d) recall. Metrics are computed across all five considered synthetic families, with $p = 10$ features.

In terms of precision (Fig. 4c), REX performs comparably well with methods like CAM and FCI, demonstrating that it avoids excessive false positives while capturing meaningful causal links. This level of precision is advantageous for applications requiring high-confidence causal relationships. However, REX’s performance in recall (Fig. 4d) is moderate, aligning closely with other methods like PC and GES, indicating that while REX is effective in identifying relevant causal relationships, it may miss some causal connections compared to approaches with higher recall like CAM.

Overall, REX demonstrates strong structural accuracy and a balanced detection capability, particularly excelling in structural precision and F1 score, which are indicative of its robustness in maintaining the validity of discovered causal structures. However, some trade-offs in recall suggest areas where further improvements could be explored to enhance REX’s sensitivity in capturing all causal connections, especially in more complex causal graphs.

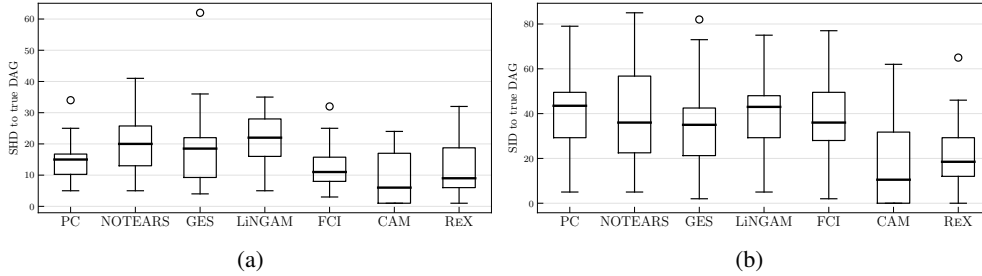


Figure 5: Benchmark between REX and compared methods for (a) SHD and (b) SID metrics.

In addition, REX achieves competitive SHD values (Fig. 5a), with a median lower than most compared methods, indicating good alignment with the true DAG structure. The variability in SHD for REX is moderate, showing some datasets where performance is comparable to CAM and FCI, while outperforming methods like LiNGAM and GES. These results suggest that REX effectively balances its structural recovery, minimizing the number of missing and extra edges across diverse scenarios.

In terms of SID, REX shows favorable performance (Fig. 5b), with lower values than most methods and a narrower interquartile range compared to GES and NOTEARS. This indicates that REX better captures interventionally relevant causal directions, providing robust predictions under interventions. While CAM achieves comparable SID performance, REX demonstrates a more consistent behavior across datasets, highlighting its adaptability to various data structures. These results confirm REX’s effectiveness in constructing causal graphs that align closely with both the observational and interventional ground truth.

5 Results with Single-cell protein network data

We apply REX to the well-studied single-cell protein-signaling network dataset, which was originally analyzed by [32] to assess the performance of structure learning methods against a largely known ground truth. This dataset, commonly referred to as *Sachs*, consists of $m = 7466$ measurements of protein concentrations for $p = 11$ proteins: Plc, Pkc, Pka, PIP2, PIP3, Raf, Mek, Erk, Akt, P38, and Jnk. For our analysis, we utilize the cleaned version of the Sachs dataset, as provided in [33], and used in [34].

Following the structure described in Sachs et al. (2005) and Ramsey and Andrews (2018), we divide the 11 variables into two tiers: Plc, Pkc, Pka, PIP2, and PIP3 are categorized into tier 1, while the remaining variables (Raf, Mek, Erk, Akt, P38, and Jnk) belong to tier 2. Grouping variables in tiers is done to represent a causal dependency (temporal) order, such that variables at a given tier (e.g., 1) are not expected to receive directed edges from those in subsequent tiers (i.e., 2, 3, . . .), but only from variables in the same or previous tiers. Hence, although feedback loops are suggested to exist within the network, they are thought to primarily occur among variables in tier 1, with no directed edges expected from tier 2 to tier 1. This prior information is added to REX and the compared methods prior to running them.

Fig. 6 shows the causal graph obtained by REX on the Sachs dataset. With a precision of 0.952, a recall of 0.471 and a F1-score of 0.629, REX is able to correctly recover important causal relationships from the data. The number of wrong edges or wrong directions are minimized, though the entire set of edges is not recovered. We note that to recover this DAG, REX was applied with exactly the same parametrization as in the synthetic datasets.

We compare REX’s performance with that of the compared methods on the Sachs dataset (Table 2). The results are based on five-runs with different seeds, all methods using parameter settings consistent with those applied to the synthetic datasets.

The results in Table 2 demonstrate that REX significantly outperforms other methods across most evaluation metrics on this dataset, achieving the highest score in precision and F1 score, indicating both high specificity and a strong balance between precision and recall. While its recall of 0.471 is moderate, it is still competitive and notably higher than that of most methods, except for CAM, which achieved a higher recall of 0.6. In terms of structural accuracy, REX also reports the lowest SHD (median of 9), implying fewer structural errors compared to others, with FCI and CAM following at 13 and 39, respectively. In addition, REX has a relatively good value for SID (median of 39),

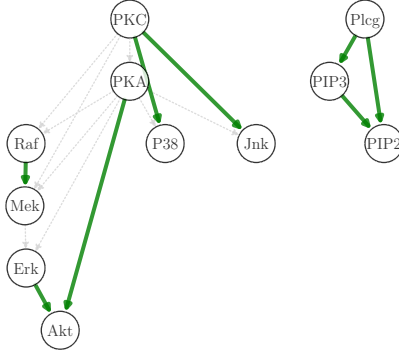


Figure 6: Plausible causal graph obtained by REX on the Sachs dataset. Green arrows correspond to correctly predicted edges, while gray arrows are true edges missed by REX.

Table 2: Summary metrics for all considered methods on the Sachs dataset.

Method	Precision	Recall	F1	SHD	SID
PC	0.462 ±0.04	0.316 ±0.05	0.376 ±0.04	15 ±2	53 ±3
FCI	0.667 ±0.05	0.421 ±0.06	0.516 ±0.05	13 ±3	36 ±4
GES	0.200 ±0.02	0.421 ±0.03	0.273 ±0.03	41 ±1	50 ±2
LiNGAM	0.115 ±0.01	0.158 ±0.02	0.134 ±0.02	37 ±1	53 ±1
NOTEARS	0.212 ±0.03	0.368 ±0.04	0.270 ±0.03	36 ±2	50 ±2
CAM	0.250 ±0.05	0.600 ±0.06	0.353 ±0.05	39 ±3	47 ±4
REX	0.952 ±0.02	0.471 ±0.01	0.629 ±0.02	9 ±1	39 ±2

indicating also a noteworthy intervention-based structure interpretation capability. Overall, REX demonstrates strong precision and structural fidelity, supporting its robustness and reliability for causal discovery in this context.

While it is possible that further tuning could improve the performance of other methods, REX achieves top scores in precision and F1 without such adjustments, highlighting its robustness and reliability in causal discovery under default settings.

6 Practical Considerations and Future Work

During the development of REX, we addressed several considerations and decisions, while also identifying potential areas for future improvement. Next, we discuss in detail topics such as opting for SHAP values over other explainability methods, the challenges of multicollinearity, and the potential for experimenting with various machine learning regressors. These factors play a crucial role in shaping the method’s performance and open up opportunities for further research to refine and enhance the proposed approach.

6.1 Explainability techniques

During method development, we compared Shapley values against other explainability techniques, such as feature importance, partial dependency plots, and LIME, and found that Shapley values outperformed all of them by a large margin. These techniques produced noisy results with limited practical application. As discussed in Section 2.1, while Shapley values may also provide insights into causal relationships, since they are not inherently causal, their application to obtain plausible causal graphs must be used in conjunction with causal inference techniques to explore and validate potential causal dynamics within the data.

6.2 Multicollinearity considerations

A significant challenge when using Shapley values for model interpretation, particularly in the context of establishing causal relationships among features in a dataset, comes from situations where some of these features are highly correlated [35]. An scenario with multicollinearity makes difficult to isolate the individual effect of each feature on the model’s predictions. In such cases, Shapley values may be argued to distribute the importance across correlated

features, potentially obscuring the true contribution of each individual feature to the model’s predictions. This distribution of importance can be understood as source of ambiguity, as it could become challenging to discern whether the impact on the prediction is due to the intrinsic value of a feature or its correlation with other features.

The implementation of Shapley values in SHAP by [4] includes model-agnostic explainers like GradientExplainer or TreeExplainer as a potential solution [36] to mitigate the effects of multicollinearity. Unlike other explainers that might treat features collectively or consider their joint distributions, interventional explainers operate under an interventional framework where the impact of each feature on the model’s output is computed independently, assuming other features remain constant. This approach aligns with the concept of partial derivatives, focusing on the sensitivity of the output to changes in each feature, treated in isolation. By doing so, interventional explainers effectively disentangle the intertwined influences of correlated features, making it easier to interpret the model in terms of causal relationships. This is particularly useful in deep learning models where the intricate interactions of features can be complex and opaque.

In the context of REX, the adoption of model-agnostic explainers is intricately linked to the type of regressor being employed. When utilizing DFN, GradientExplainer is chosen, tailored to capture the complex, layered interactions and non-linear mappings characteristic of these models. Conversely, when employing Gradient Boosting Trees, TreeExplainer is utilized as it is more suited to dissecting the sequential, decision-tree-based learning process intrinsic to these algorithms. This adaptability in the choice of explainers is crucial, as it ensures that the explanations generated are not only robust but also appropriately aligned with the underlying mechanics of the chosen regression model.

6.3 Future Work

As discussed in Section 3.1, a key direction for future research is the investigation of alternative regressors beyond the deep feed-forward neural networks (DFN) and gradient boosting trees (GBT) used in this study. Both models support SHAP, enabling interpretability of their predictions. However, other machine learning models that also facilitate SHAP explainability could be integrated into the REX framework. For instance, Lasso-based methods, such as Group Lasso [37], commonly used in causal discovery approaches like CAM [14], offer inherent sparsity. This property may enhance interpretability by reducing irrelevant connections, potentially yielding more interpretable causal graphs. SHAP compatibility with these methods positions them as promising candidates for future integration into REX.

Further exploration could also include models like Elastic Net regression [38], which combines the sparsity of Lasso with the regularization of Ridge regression, possibly improving feature selection while retaining SHAP explainability. Tree-based ensemble methods such as CatBoost and LightGBM, which have native SHAP support, also present an attractive alternative to GBTs, potentially offering computational advantages on large datasets. Expanding REX to incorporate these alternatives could enhance its adaptability and performance across various data structures and application contexts.

Another research area for REX is its application to datasets with distributional shifts, where the data-generating process may vary across different populations or over time. Recent work [39] has addressed this challenge by identifying features that remain causally invariant across changing distributions. Integrating such principles into the REX could enhance its applicability to real-world datasets where the assumption of consistent distributions does not hold, improving its robustness and generalization capability.

Exploring the behavior of the different SHAP values of Equation (3) in each of the S subsets may provide more information on how the variables are grouped together within a larger causal structure. Relating this future analysis to techniques that give us information about how they are grouped may help us better discern relationships between nodes so that we can distinguish between parents and ancestors.

Additionally, efforts could be made to refine the model’s scalability and enhance its ability to handle larger datasets and higher-dimensional graphs.

7 Conclusion

In this paper, we introduced REX, a novel causal discovery method that leverages machine learning and Shapley-based explainability to address key challenges in uncovering causal structures, particularly in complex and nonlinear datasets. The approach combines interventional explainers to compute Shapley values with a bootstrapping mechanism, followed by an Additive Noise Model (ANM) for edge orientation. A novel SHAP discrepancy measure further refines the causal graph by quantifying the agreement between Shapley values and their associated features, filtering out spurious relationships.

Our experiments on five families of synthetic datasets and the Sachs single-cell protein-signaling dataset [32] illustrate the effectiveness and robustness of REX. Not only does it recover causal relationships with high precision and low orientation error, but it also compares favorably with existing state-of-the-art methods. By providing interpretable insights into the underlying causal dynamics, REX enables contrasting inferred causal links with domain expertise.

We highlight three major strengths of REX. First, its results are comparable to leading causal discovery methods across varying nonlinearities. Second, the use of Shapley values brings a valuable layer of interpretability, fostering trust and supporting evidence-based decisions. Third, the integration of data-driven modeling, explainability, and a bootstrapping mechanism provides robustness against spurious edges and orientation errors. However, the computational cost of calculating Shapley values in high-dimensional settings remains a key limitation, prompting future work on scalable, approximate solutions and more efficient architectures. Ongoing advances in GPU computing or distributed ML can significantly help to mitigate the scalability limitation in future implementations.

Looking ahead, we see potential for extending REX in multiple directions (see Section 6.3). Investigating its performance under distributional shifts, employing ensemble SHAP strategies to mitigate collinearity issues, and adopting computational frameworks that handle large or streaming datasets will further broaden its applicability. Moreover, integrating domain-specific priors and exploring advanced regressors such as Lasso-based or alternative tree-based ensemble implementations could further enhance performance and interpretability.

In fields like healthcare, finance, and economics, where reliable causal insights are crucial, REX’s interpretability is especially beneficial. We encourage the community to adopt and adapt REX for a wide range of applications, and have made all code and datasets publicly available at <https://github.com/renero/causalgraph>. Through such collaborations, we anticipate continued progress in interpretable causal discovery, ultimately advancing our ability to unravel complex causal relationships across diverse domains.

Acknowledgements

This work has been partially supported by a Ramon y Cajal contract (RYC2019-028578-I), a Gipuzkoa Fellows grant (2022-FELL-000003-01), and a grant from the Spanish MCIN (PID2021-126718OA-I00).

References

- [1] Judea Pearl. *Causality: Models, Reasoning, and Inference*. Cambridge University Press, 2 edition, 2009.
- [2] Peter Spirtes, Clark Glymour, and Richard Scheines. *Causation, Prediction, and Search*. MIT Press, 2 edition, 2000.
- [3] Jonas Peters, Dominik Janzing, and Bernhard Schölkopf. *Elements of Causal Inference: Foundations and Learning Algorithms*. Adaptive Computation and Machine Learning. MIT Press, Cambridge, MA, 2017.
- [4] Scott M Lundberg and Su-In Lee. A unified approach to interpreting model predictions. In *Advances in Neural Information Processing Systems*, pages 4765–4774, 2017.
- [5] Lloyd S Shapley. A value for n-person games. In Harold W. Kuhn and Albert W. Tucker, editors, *Contributions to the Theory of Games*, volume 2, pages 307–317. Princeton University Press, 1953.
- [6] Anupam Datta, Shayak Sen, and Yair Zick. Algorithmic transparency via quantitative input influence: Theory and experiments with learning systems. In *2016 IEEE Symposium on Security and Privacy (SP)*, pages 598–617. IEEE, 2016.
- [7] Mukund Sundararajan and Amir Najmi. The many shapley values for model explanation. In *International Conference on Machine Learning*, pages 9269–9278. PMLR, 2019.
- [8] Bernhard Schölkopf. *Causality for Machine Learning*, page 765–804. Association for Computing Machinery, New York, NY, USA, 1 edition, 2022.
- [9] Grégoire Montavon, Wojciech Samek, and Klaus-Robert Müller. Methods for interpreting and understanding deep neural networks. *Digital Signal Processing*, 73:1–15, 2018.
- [10] Kun Zhang, Yoshua Bengio, and Bernhard Schölkopf. Learning causality and causality-related learning: some recent progress. *National Science Review*, 7(1):26–28, 2020.
- [11] Peter Spirtes, Christopher Meek, and Thomas Richardson. Causal discovery in the presence of latent variables and selection bias. *Computation, Causality, and Discovery*, pages 211–252, 1999.
- [12] David Maxwell Chickering. Optimal structure identification with greedy search. *Journal of machine learning research*, 3(Nov):507–554, 2002.

- [13] Shohei Shimizu, Patrik O Hoyer, Aapo Hyvärinen, and Antti Kerminen. A linear non-gaussian acyclic model for causal discovery. *Journal of Machine Learning Research*, 7(Oct):2003–2030, 2006.
- [14] Peter Bühlmann, Jonas Peters, and Jan Ernest. CAM: Causal additive models, high-dimensional order search and penalized regression. *The Annals of Statistics*, 42(6):2526–2556, 2014.
- [15] Ioannis Tsamardinos, Laura E Brown, and Constantin F Aliferis. The max-min hill-climbing bayesian network structure learning algorithm. *Machine Learning*, 65(1):31–78, 2006.
- [16] Xun Zheng, Bryon Aragam, Pradeep K Ravikumar, and Eric P Xing. Dags with no tears: Continuous optimization for structure learning. *Advances in neural information processing systems*, 31, 2018.
- [17] Diviyani Kalainathan and Olivier Goudet. SAM: Structural agnostic model, causal discovery and penalized adversarial learning. In *Proceedings of the 22nd International Conference on Artificial Intelligence and Statistics (AISTATS)*, pages 10–19. PMLR, 2019.
- [18] Yue Yu, Jie Chen, Tian Gao, and Mo Yu. DAG-GNN: DAG structure learning with graph neural networks. In *International Conference on Machine Learning*, pages 7154–7163. PMLR, 2019.
- [19] Tom Heskes, Evi Sijben, Ioan Gabriel Bucur, and Tom Claassen. Causal shapley values: Exploiting causal knowledge to explain individual predictions of complex models. *Advances in neural information processing systems*, 33:4778–4789, 2020.
- [20] Chao Min, Guoquan Wen, Liangjie Gou, Xiaogang Li, and Zhaozhong Yang. Interpretability and causal discovery of the machine learning models to predict the production of CBM wells after hydraulic fracturing. *Energy*, page 129211, 2023.
- [21] G Xu, TD Duong, Q Li, S Liu, and X Wang. Causality learning: A new perspective for interpretable machine learning. *IEEE Intelligent Informatics Bulletin*, 2020.
- [22] Sisi Ma and Roshan Tourani. Predictive and causal implications of using shapley value for model interpretation. In *Proceedings of the 2020 KDD workshop on causal discovery*, pages 23–38. PMLR, 2020.
- [23] Kurt Hornik, Maxwell Stinchcombe, and Halbert White. Multilayer feedforward networks are universal approximators. *Neural networks*, 2(5):359–366, 1989.
- [24] Jerome H Friedman. Greedy function approximation: A gradient boosting machine. *Annals of statistics*, pages 1189–1232, 2001.
- [25] James Bergstra, Rémi Bardenet, Yoshua Bengio, and Balázs Kégl. Algorithms for hyper-parameter optimization. *Advances in neural information processing systems*, 24, 2011.
- [26] Boxiang Zhao, Shuliang Wang, Lianhua Chi, Hanning Yuan, Ye Yuan, Qi Li, Jing Geng, and Shao-Liang Zhang. Coresets for fast causal discovery with the additive noise model. *Pattern Recognition*, 148:110149, 2024.
- [27] Arthur Gretton, Kenji Fukumizu, Choon Teo, Le Song, Bernhard Schölkopf, and Alex Smola. A kernel statistical test of independence. *Advances in neural information processing systems*, 20, 2007.
- [28] Arthur Gretton and László Györfi. Consistent nonparametric tests of independence. *The Journal of Machine Learning Research*, 11:1391–1423, 2010.
- [29] Diviyani Kalainathan. *Generative Neural Networks to infer Causal Mechanisms : algorithms and applications*. Theses, Université Paris Saclay (COMUE), December 2019.
- [30] Jonas Peters, Joris M. Mooij, Dominik Janzing, and Bernhard Schölkopf. Causal discovery with continuous additive noise models. *J. Mach. Learn. Res.*, 15(1):2009–2053, January 2014.
- [31] Jonas Peters and Peter Bühlmann. Structural Intervention Distance for Evaluating Causal Graphs. *Neural Computation*, 27(3):771–799, 03 2015.
- [32] Karen Sachs, Omar Perez, Dana Pe’er, Douglas A Lauffenburger, and Garry P Nolan. Causal protein-signaling networks derived from multiparameter single-cell data. *Science*, 308(5721):523–529, 2005.
- [33] Joseph D. Ramsey and Bryan Andrews. FASK with interventional knowledge recovers edges from the sachs model. *CoRR*, abs/1805.03108, 2018.
- [34] Ting-Hsuan Chang, Zijian Guo, and Daniel Malinsky. Post-selection inference for causal effects after causal discovery, 2024.
- [35] Dominik Janzing, Lenon Minorics, and Patrick Bloebaum. Feature relevance quantification in explainable AI: A causal problem. In *Proceedings of the Twenty Third International Conference on Artificial Intelligence and Statistics*, pages 2907–2916, June 2020. ISSN: 2640-3498.

- [36] Hugh Chen, Joseph D. Janizek, Scott Lundberg, and Su-In Lee. True to the Model or True to the Data?, June 2020. arXiv:2006.16234 [cs, stat] version: 1.
- [37] Ming Yuan and Yi Lin. Model selection and estimation in regression with grouped variables. *Journal of the Royal Statistical Society: Series B (Statistical Methodology)*, 68(1):49–67, 2006.
- [38] Hui Zou and Trevor Hastie. Regularization and variable selection via the elastic net. *Journal of the Royal Statistical Society: Series B (Statistical Methodology)*, 67(2):301–320, 2005.
- [39] Yujie Wang, Kui Yu, Guodu Xiang, Fuyuan Cao, and Jiye Liang. Discovering causally invariant features for out-of-distribution generalization. *Pattern Recognition*, 150:110338, 2024.

Appendices

A Parents selection example

Fig. 7 illustrates how the parents selection described in Algorithm 2 mechanism works. On panel (a) there is a significant shift between the features that are more influential ($V1$ and $V2$) and the rest. On panel (b), such shift is not so clear, though the first group of three ($V0$, $V2$ and $V4$) present a more pronounced influence than the rest. On top of each plot, the variables selected by Algorithm 2 are written to the right of the target variable, as parents (\leftarrow) of the target.

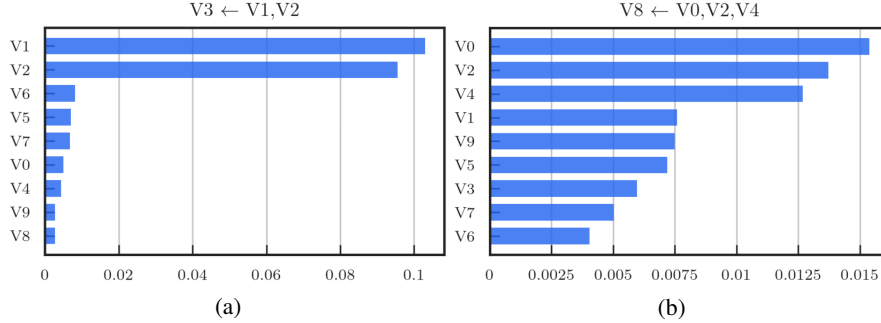


Figure 7: Example of SHAP values (x-axis) for: (a) endogenous variable $V3$; and (b) $V8$.

In some cases, the proposed Algorithm 2 might discard features that are influential on the outcome of the regression of the target variable. This would be the case for example if, in Fig.7b, only the first variable $V0$ is selected instead of the first three variables (i.e., $V0$, $V2$ and $V4$). In those cases, manual supervision or special parametrization of the method would be required to ensure that the selected features are also the most influential. Indeed, an additional parametrization of Algorithm 2 allows to run the method in *greedy* mode, to return not only the features with higher impact but all whose value is above a given percentile of the distribution of SHAP values. This tuning can be automatically activated in those cases where the feature selection process leads to a plausible causal graph (Section 3.2.3) with a number of edges significantly below the max number of edges expected in a fully connected DAG, given by $\frac{p(p-1)}{2}$. We note that none of the experimental results described in Section 4 required the use of this or any other special parametrization of the main REX method.

B SHAP discrepancy example

Fig. 8 illustrates the role of SHAP values and the discrepancy between two potential causes or parent features X_j , and one effect or dependent feature X_i .

In (b) we can see discrepancy values for V_4 versus V_3 (is V_3 a direct cause of V_4 ?), showing a low discrepancy value $\delta_{ij}^{(t)} = 0.08$, consistent with the fact that V_4 is a direct child of V_3 . (c) shows that V_6 could also be considered a direct cause of V_4 . However, in (d) we can also check that V_4 could also be considered a direct cause of V_6 . In (e) we can check how V_5 present a very high discrepancy (1.99), indicating that V_5 should be discarded among the potential parents of V_4 .

The low SHAP discrepancy values for causally related variables support the ability of SHAP discrepancy to distinguish causal dependencies, whereas the high discrepancy for non-causal relationships ($V_4 \rightarrow V_5$) demonstrates its effectiveness in filtering out irrelevant connections.

C Performance comparison between single and combinations of regressors

REX employs two regressors—DFN and GBT—to obtain individual causal graphs from the data (see Section 3.1). The final DAG is constructed by combining these graphs using a union (\cup) operation. This operation effectively includes all edges identified by either regressor, ensuring that any edge detected by at least one of them is incorporated into the final solution. This approach aims to leverage the strengths of both regressors, capturing edges that might be missed by one but detected by the other.

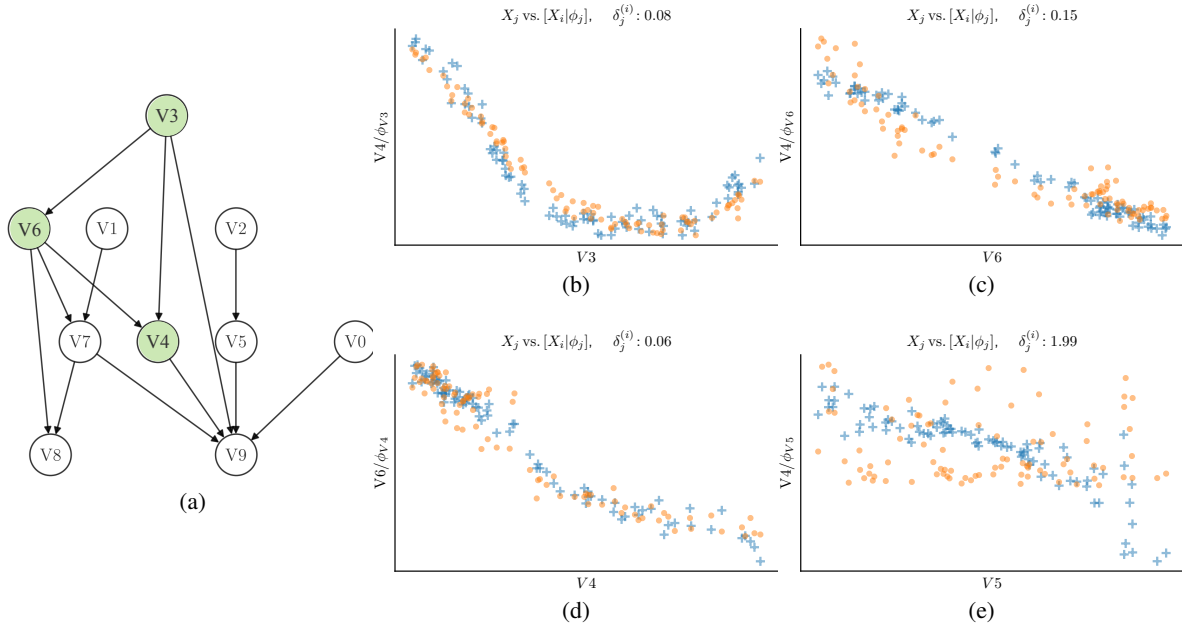


Figure 8: (a) Ground truth DAG for a system of 10 variables (V_0 to V_9). Highlighted in green are nodes V_3 , V_4 , and V_6 , which are either direct or indirect causes or effects of one another. (b)-(e) SHAP discrepancy analysis for variable pairs in the graph. As observed, discrepancy values between pairs of V_3 , V_4 , and V_6 are low ((b), (c) and (d)), in contrast to the one obtained when analyzing the pair V_4 , V_5 (e).

Experiments on the synthetic datasets proposed in this study (see Section 4) indicate that this combined approach results in better predictive performance than using the output of a single regressor (Fig. 9). Specifically, the union of the regressors’ outputs yields higher F1 scores across datasets with 10, 15, 20 and 25 variables, suggesting a more accurate recovery of the true causal structures. DFN’s F1 is 0.577 and GBT’s F1 is 0.59, while union’s F1 is 0.712, a 23.4% higher.

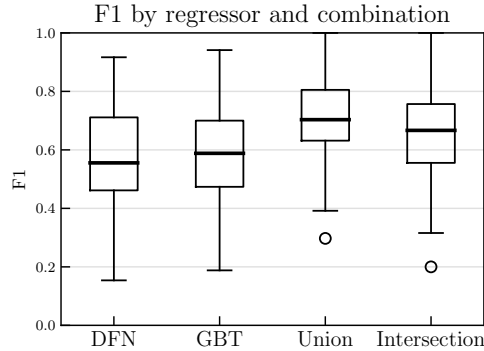


Figure 9: REX’s F1 scores for all synthetic datasets with 10, 15, 20 and 25 variables, comparing the DAGs obtained by a single regressor (DFN or GBT) to those obtained by combining them through union (\cup) and intersection (\cap) operations.

In addition to the union operation, we have also tested the intersection (\cap) operation for combining the regressors’ outputs. This method includes only the edges that are identified by both regressors. While the intersection approach also provides better results than using either regressor individually, its performance is slightly inferior (0.667) to that of the union operation (4.9% lower). The more conservative nature of the intersection may exclude some true causal edges identified by only one regressor, leading to a less comprehensive causal graph.

D Sample DAGs

In this section, a number of sample DAGs are presented to illustrate the differences between the output DAG of the proposed method REX and the ones from the comparison methods.

Fig. 10 and 11 show sample DAGs generated from a Gaussian additive and Sigmoid additive processes, respectively, with $p = 10$ variables. Solid green edges represent correctly predicted causal relationships that match the ground truth, light gray dotted lines indicate edges that were present in the ground truth but not predicted by the method, dashed orange lines represent edges where the causal pair was correctly identified but with the wrong direction, and red dash-dot lines correspond to incorrectly predicted edges.

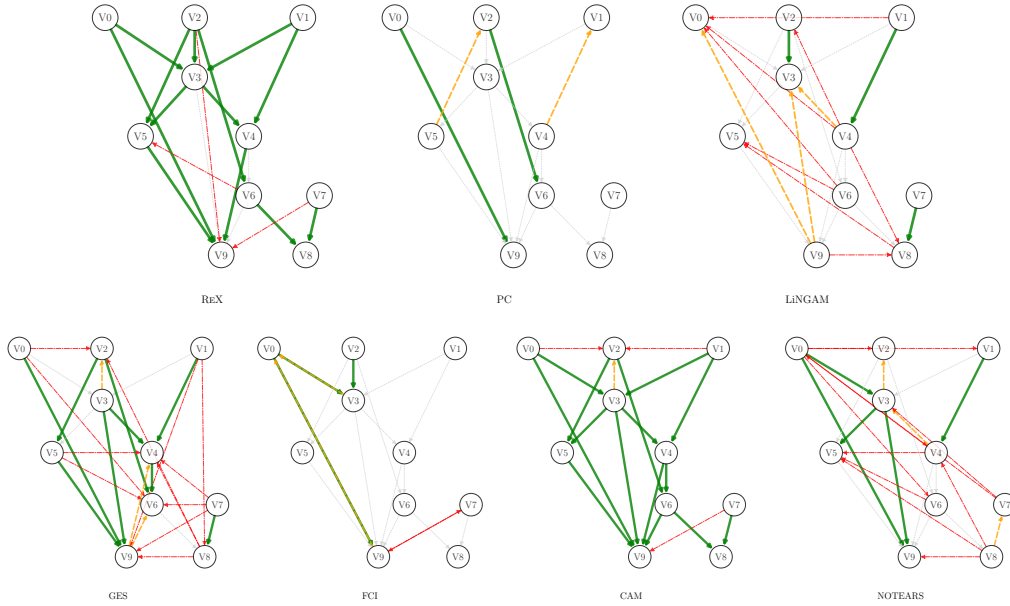


Figure 10: Sample DAGs generated from a Gaussian additive process.

In Fig. 10, REX outperforms the other methods by achieving a higher proportion of correctly oriented causal edges (solid green), particularly in areas with more complex relationships, such as nodes V_3 , V_4 , and V_6 . Moreover, REX demonstrates a lower number of incorrect predictions (red dash-dot lines) and fewer reversed causal directions (dashed orange) compared to methods like LiNGAM and GES, which show more frequent orientation errors. This highlights REX’s ability to both recover true causal relationships and accurately predict their direction, even in challenging scenarios.

In Fig. 11, REX method continues to demonstrate strong performance by recovering a larger number of true causal relationships (solid green lines) compared to other methods. Notably, REX accurately captures relationships involving nodes V_3 , V_4 , and V_6 , while methods like PC, LiNGAM, and GES tend to miss several true edges or predict a higher number of reversed causal directions (dashed orange lines). Furthermore, REX shows fewer incorrect predictions (red dash-dot lines) relative to CAM and FCI, both of which exhibit a greater number of spurious connections. This highlights REX’s robustness in discovering complex causal structures and correctly orienting edges, particularly in this dataset where sigmoid additive relationships present a more challenging structure.

E Additional results

Here we provide additional results of REX for the five considered families of synthetic datasets and the different values of input features p .

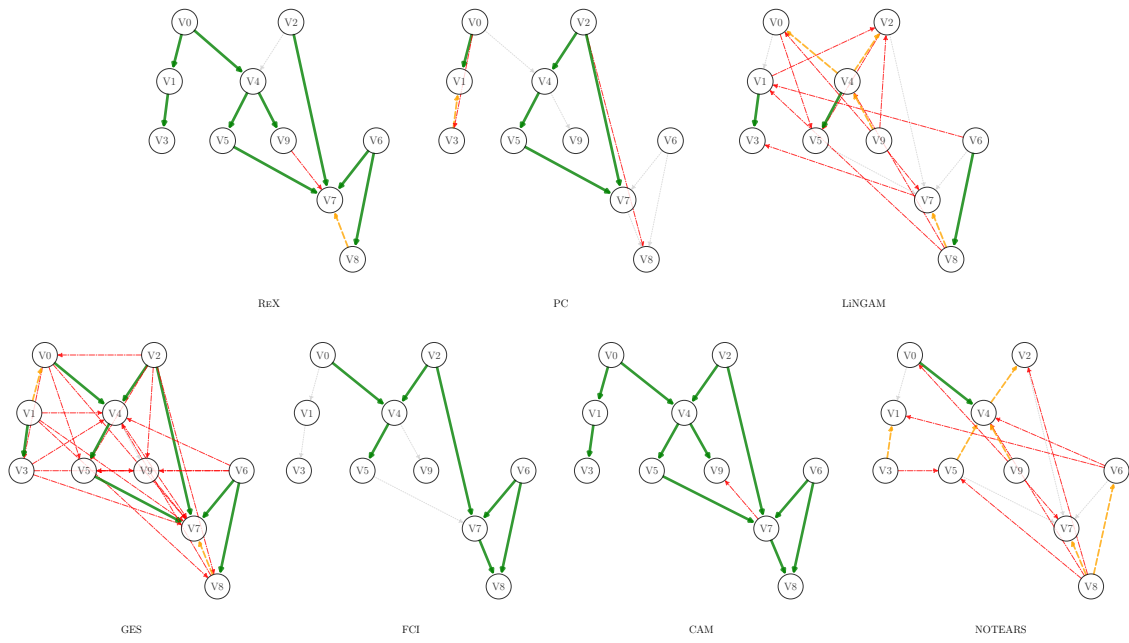


Figure 11: Sample DAGs generated from a Sigmoid additive process.

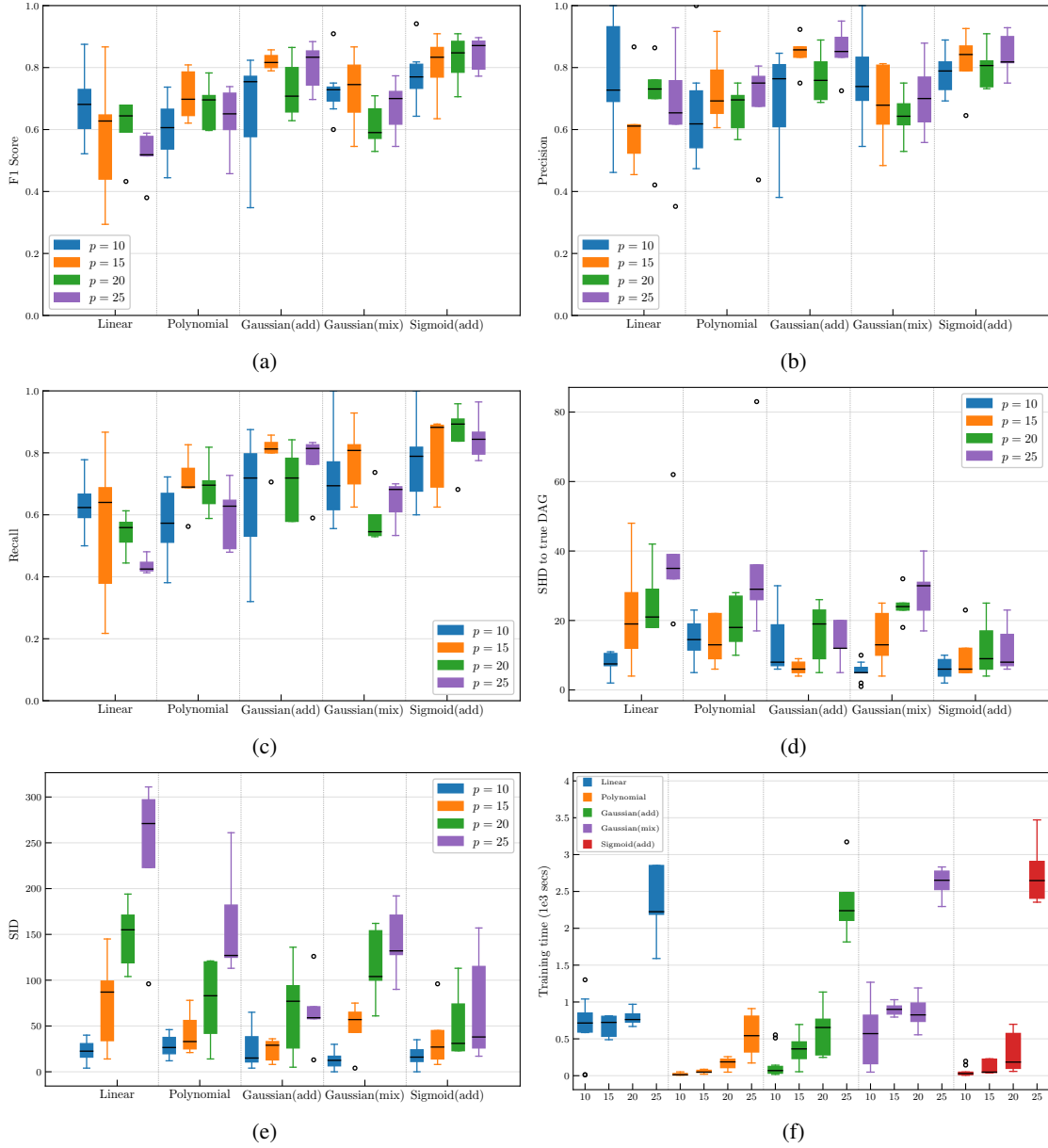


Figure 12: F1 (a), Precision (b), Recall (c), SHD (d) and SID (e) for REX as a function of the number of features and synthetic data generation mechanism. Panel (f) represents the training time for the different families of synthetic data and number of variables used (x-axis).